

**Tropospheric
distribution of
sulphate aerosol**

S. Verma et al.

Tropospheric distribution of sulphate aerosol mass and number concentration during INDOEX-IFP and its transport over the Indian Ocean: a GCM study

S. Verma¹, O. Boucher², M. S. Reddy², S. K. Deb¹, H. C. Upadhyaya¹, P. Le Van³, F. S. Binkowski⁴, and O. P. Sharma¹

¹Centre for Atmospheric Sciences, Indian Institute of Technology Delhi, New Delhi, India

²Laboratoire d'Optique Atmosphérique, CNRS/Université des Sciences et Technologies de Lille, 59655 Villeneuve d'Ascq Cedex, France

³Laboratoire de Météorologie Dynamique, Ecole Normale Supérieure, 24 rue Lhomond, 75231 Paris Cedex 05, France

⁴Environmental Science and Engineering, University of North Carolina, Chapel Hill, USA

Received: 11 October 2004 – Accepted: 22 October 2004 – Published: 31 January 2005

Correspondence to: O. P. Sharma (opsharma@cas.iitd.ac.in)

© 2005 Author(s). This work is licensed under a Creative Commons License.

Title Page

Abstract

Introduction

Conclusions

References

Tables

Figures

◀

▶

◀

▶

Back

Close

Full Screen / Esc

Print Version

Interactive Discussion

EGU

Abstract

An interactive sulphate aerosol chemistry module has been incorporated in the Laboratoire de Météorologie Dynamique General Circulation Model (LMD-GCM) to simulate the sulphur chemistry during the Indian Ocean Experiment (INDOEX) Intensive Field Phase-1999 (INDOEX-IFP). The originality of this module is its ability to predict particle mass and number concentration for the Aitken and accumulation modes. The model qualitatively reproduces the spatial patterns of observations on sulphate aerosol during INDOEX. On the basis of size distribution retrieved from the observations made along the cruise route during 1998 and 1999, the model successfully simulates the order of magnitude and the general north-south gradient in aerosol number concentration. The result shows the southward migration of minimum concentrations, which follows ITCZ (Inter Tropical Convergence Zone) migration. Sulphate surface concentration during INDOEX-IFP at Kaashidhoo (73.46° E, 4.96° N) gives an agreement within a factor of 2 to 3. Predicted sulphate aerosol optical depth (AOD) matches reasonably with measured values, indicating the capability of this model to predict the vertically integrated column sulphate burden. The Indian contribution to estimated sulphate burden over India is more than 60% with values upto 40% over the Arabian Sea.

1. Introduction

The aerosol effects on climate can be large and complex due to the fact that aerosols chemical composition, abundance and size distribution are highly variable, both spatially and temporally. Most of the earliest investigations on direct aerosol forcing have focused on sulphate aerosols because of their importance as an anthropogenic aerosol component (Charlson et al., 1992; Kiehl and Briegleb, 1993). Sulphate aerosols are capable of modifying the climate not only by scattering incoming sunlight back to space (direct effect) but also by altering the properties of clouds (indirect effect). In order to further understand sulphate aerosol-climate interactions, the present study is carried

Tropospheric distribution of sulphate aerosol

S. Verma et al.

Title Page

Abstract

Introduction

Conclusions

References

Tables

Figures

◀

▶

◀

▶

Back

Close

Full Screen / Esc

Print Version

Interactive Discussion

out with the Laboratoire de Météorologie Dynamique global model to produce the simulation of INDOEX-IFP. The sulphate aerosol/chemistry is interactively included in the model. The three fundamental objectives of this study are

1. to develop a tool for simulating sulphate aerosol dynamics,
2. to compare and evaluate model-derived physical, optical, and radiative properties of sulphate aerosols with observations during INDOEX-IFP,
3. to examine sulphate aerosol transport and radiative forcing, and the contribution of Indian emissions to the regional burden using the emission inventory developed by [Reddy and Venkataraman \(2002a,b\)](#).

INDOEX was conducted during the winter monsoon season, when pristine air-mass from the southern hemisphere and not-so-clean air from the Indian subcontinent meet over the tropical Indian Ocean and provide a natural laboratory for studying aerosol influences. Primarily, its goal was to assess the natural and anthropogenic climate forcing due to aerosols and to examine the underlying feedback mechanisms on scales relevant to regional and global climate. [Ramanathan et al. \(2001\)](#) have presented the INDOEX results for the oceanic regions adjacent to the Indian subcontinent, which reveal the presence of a dense anthropogenic aerosol layer over China, South and Southeast Asia. While INDOEX suggests south/southeast Asia as the regions of major sources of aerosols for the Indian Ocean, the controversy still persists regarding the formation, movement, persistence and effects of this regional haze on the regional and global climate (the South Asian Atmospheric Brown Cloud) ([UNEP and C⁴, 2002](#)). In order to address such high priority issues of concern to climate change, this study, in logical continuation of earlier studies ([Krishnamurthy et al., 1998](#); [Rajeev et al., 2000](#); [Satheesh and Ramanathan, 2000](#); [Verver et al., 2001](#); [Rasch et al., 2001](#); [Ramanathan et al., 2001](#)), deals with the INDOEX region. An attempt has been made here to reproduce the observed variations in the sulphate aerosol mass and number concentration during the Indian Ocean Experiment from January to March 1999. The unique aspects of this study are the following:

**Tropospheric
distribution of
sulphate aerosol**

S. Verma et al.

Title Page

Abstract

Introduction

Conclusions

References

Tables

Figures

◀

▶

◀

▶

Back

Close

Full Screen / Esc

Print Version

Interactive Discussion

**Tropospheric
distribution of
sulphate aerosol**S. Verma et al.

(i) In most of the global sulphur models only sulphate mass is estimated as a prognostic variable. The number concentration is inferred assuming a constant size distribution. In contrast, in our implementation the sulphate number concentration is also treated as a prognostic variable. The knowledge of the sulphate aerosol number concentration is important to understand the indirect radiative forcing of the aerosols and to refine estimates of the direct radiative forcing.

(ii) A comprehensive scheme, where the concentrations of radicals like OH, HO₂ and gases like O₃, H₂O₂, NH₃ and NO_x are computed within the GCM, is introduced in the zoom version (LMDZ) of LMD-GCM.

2. Model description

2.1. The atmospheric global model

The LMDZ is a development of previous LMD model described by [Sadourny and Laval \(1984\)](#), which was utilised along with other global models of major meteorological centres, to achieve the AMIP I objective of atmospheric model intercomparison ([Boer, 1992](#); [Cess et al., 1989](#)) and also to carry out long-term simulations for certain climate and aerosol studies ([Le Treut et al., 1994](#); [Boucher and Lohmann, 1995](#); [Sharma et al., 1998](#); [Boucher et al., 1998, 2002](#), etc.). The LMDZ has the capability to zoom with a finer resolution over a specific region of interest over the globe and relatively a coarser resolution over rest of the globe, which gives a unique opportunity to study the regional aspects of aerosols. The model solves the primitive equations of meteorology and mass continuity for fifteen tracers viz., dimethylsulphide (DMS), hydrogensulphide (H₂S), dimethylsulphoxide (DMSO), methanesulphonic acid (MSA), sulphur dioxide (SO₂), nitrogen oxides (NO_x), carbon monoxide (CO), ozone (O₃), hydrogen peroxide (H₂O₂), sulphate aerosol mass and number for Aitken and accumulation modes, water vapour, and liquid water. The discrete analogues of the dynamical equations are obtained using finite difference formulations on Arakawa-C grid and the physical pack-

[Title Page](#)[Abstract](#)[Introduction](#)[Conclusions](#)[References](#)[Tables](#)[Figures](#)[◀](#)[▶](#)[◀](#)[▶](#)[Back](#)[Close](#)[Full Screen / Esc](#)[Print Version](#)[Interactive Discussion](#)

EGU

**Tropospheric
distribution of
sulphate aerosol**S. Verma et al.

[Title Page](#)[Abstract](#)[Introduction](#)[Conclusions](#)[References](#)[Tables](#)[Figures](#)[◀](#)[▶](#)[◀](#)[▶](#)[Back](#)[Close](#)[Full Screen / Esc](#)[Print Version](#)[Interactive Discussion](#)

EGU

age of the model includes a set of parameterisations for convection, radiative transfer, planetary boundary layer (PBL), gravity wave drag and ground hydrology with no vegetation. For a complete description of the atmospheric model dynamics and physical parameterisation of physical processes one may refer to [Sadourny and Laval \(1984\)](#), [Le Treut et al. \(1994\)](#) and [Hourdin and Armengaud \(1999\)](#). The climatology of this model has been presented by [Li \(1999\)](#) and [Lott \(1999\)](#). An important addition to LMDZ in the version used here is the inclusion of a prognostic sulphur-cycle scheme. Except for some parameterisations, it should be noted that the chemistry module has been developed independently from that of [Boucher et al. \(2002\)](#) and [Hauglustaine et al. \(2004\)](#).

2.2. Chemistry and aerosol modules

2.2.1. Gas phase chemistry

The chemistry module includes natural and anthropogenic emissions, treatment of sulphur and nitrogen sources, their chemical transformations and deposition processes. The basic chemistry module consists of 21 most important reactions in the gas-phase comprising the photolytic dissociations of O_3 , formaldehyde (HCHO), H_2O_2 , NO_x and DMS. The gas phase reactions and reaction rates are those described in [Chen and Crutzen \(1994\)](#) and [Lawrence et al. \(1999\)](#). The parameterisation of DMS oxidation has been constructed assuming that DMS reacts only with OH, ignoring its reaction with NO_3 and other species. DMS is oxidised by OH radical producing SO_2 and DMSO, which is further oxidised to produce SO_2 and MSA. The reactions and reaction rates for DMS are prescribed from [Atkinson et al. \(1989\)](#) and [Chatfield and Crutzen \(1990\)](#). The gas phase reactions with corresponding rates are presented in Table 1. It calculates the concentration of hydroxyl radicals (OH, HO_2) – which act as important oxidising agents to convert sulphur dioxide to sulphuric acid in vapour form by series of chain reactions initiated by them. It is worthwhile to mention here that along with OH and HO_2 , the model also predict H_2O_2 and O_3 concentrations which have a role in aqueous-phase

2.2.2. Aqueous phase chemistry

The gas phase concentrations of SO₂, H₂O₂ and O₃ are estimated in the cloud phase assuming Henry's law and used to calculate the amount of sulphate formed in the cloudy regions. While the sulphuric acid produced by gas phase oxidation is split into two parts: one going into Aitken and the other one condensing onto the existing particles (accumulation mode) as described in Sect. 2.2.3, the sulphate produced by aqueous phase oxidation remains dissolved in cloud droplets. However, when the clouds disappear, the sulphate in the dissolved state is added to the accumulation mode mass. Therefore all new sulphate mass produced by aqueous production is added to the accumulation mode but the number of accumulation mode particles remains unchanged (Fig. 1). The model represents a simplified version of the aqueous model of Walcek and Taylor (1986) and is similar to an earlier equilibrium model of Ohta et al. (1981). The equations for chemical equilibrium of the SO₂-NH₃-CO₂-HNO₃-H₂O system are those from Chen and Crutzen (1994). The rates for aqueous phase reactions are given in Table 2. For the solution of chemical reactions (Tables 1 and 2), the model uses a numerical method (Hesstvedt et al., 1978) giving the forward time concentration as

$$C(t + \Delta t) = \frac{P}{L} + \left[C(t) - \frac{P}{L} \right] \exp(-L \Delta t) \quad (1)$$

$C(t)$ denotes the concentration of species at time t . P is the production term (molec cm⁻³ s⁻¹) and L denotes the loss rate (s⁻¹) of the chemical species. Note that a set of very stiff equations can be efficiently handled by the expression (Eq. 1). In the present model the gas phase reactions are evaluated for 30 min time step with the above-mentioned scheme. Because the reaction rates of aqueous O₃ with SO₂ are pH dependent, the 30 min time step is split into 15 time steps of 2 min each, for which the oxidation reaction rates and the cloud pH are computed (Boucher et al., 2002; Snider and Vali, 1994; Hegg and Hobbs, 1981).

Tropospheric distribution of sulphate aerosol

S. Verma et al.

Title Page

Abstract

Introduction

Conclusions

References

Tables

Figures

◀

▶

◀

▶

Back

Close

Full Screen / Esc

Print Version

Interactive Discussion

2.2.3. Aerosol module

The aerosol module of this model, based on the particle transport model of Binkowski and Shankar (1995), is also a part of Model-3 of U.S. Environment Protection Agency (EPA). The present approach utilises sulphuric acid produced in the gas phase as an input to the aerosol module which calculates aerosol mass and number density. In the aerosol model, the size distribution of sub-micron particles is represented by two overlapping lognormal distributions (Eq. 2). The two modes correspond to the particles with diameter less than $2.5\ \mu\text{m}$ (PM_{2.5}) and are called the nucleation (Aitken) and accumulation modes. The Aitken mode includes particles up to $0.1\ \mu\text{m}$ diameter while the accumulation mode covers the range from 0.1 to $2.5\ \mu\text{m}$.

$$n(\ln D) = \frac{N}{\sqrt{2\pi} \ln \sigma_g} \exp \left[-0.5 \left(\frac{\ln \frac{D}{D_g}}{\ln \sigma_g} \right)^2 \right] \quad (2)$$

where D is the particle diameter, D_g and σ_g are the geometric mean diameter and geometric standard deviation, respectively. The values of σ_g are fixed at 1.6 (Aitken mode) and 2.0 (accumulation mode). The module includes growth due to the addition of new mass, as well as the formation of new particles (Harrington and Kreidenweis, 1998a,b; Kulmala et al., 1998) from gas phase reactions (nucleation). Coagulation rate for the Aitken and accumulation mode is calculated using Gauss-Hermite numerical quadrature. Both intramodal and intermodal coagulations are considered for particle growth. For each mode, three integral properties are calculated viz., the total particle number concentration, the total surface area concentration and the total mass concentration. A detailed description of this aerosol module may be found in Binkowski and Roselle (2003). To compare the model results in terms of number and mass within the size intervals bounding the two modes, it is necessary to treat both number and mass for each mode separately as prognostic variables in the model. This model therefore

Title Page

Abstract

Introduction

Conclusions

References

Tables

Figures

◀

▶

◀

▶

Back

Close

Full Screen / Esc

Print Version

Interactive Discussion

treats aerosol mass and number in Aitken mode, and aerosol mass and number in accumulation mode as individual tracers.

2.3. Dry and wet deposition

Dry deposition is parameterised through deposition velocities, which are prescribed for each chemical species and surface types. The model uses a simple parameterisation scheme, which assumes that the rate of deposition at the surface is directly proportional to the mixing ratio (i.e., concentration) of the respective species in the lowest model layer. The flux to the surface f_d ($\text{kg m}^{-2} \text{s}^{-1}$) is expressed as:

$$f_d = \rho_{air} \mu_s v_d \quad (3)$$

where, ρ_{air} is the density of air (kg m^{-3}), μ_s is the mixing ratio of species (kg per kg of air) and v_d is the dry deposition velocity (m s^{-1}) which was prescribed depending upon the chemical constituents and the underlying surface (Table 3). The wet removal scheme considers two processes, in-cloud and below-cloud scavenging. Rainfall is computed at every time step in the GCM. Removal of gases and aerosols by rain was parameterised using the model generated precipitation formation rate following Giorgi and Chameides (1986). The scavenging rate, S_{in} (s^{-1}) is given by:

$$S_{in} = \phi f_c F_{aq} \quad (4)$$

where, ϕ is the rate of conversion of cloud water to rainwater ($\text{kg kg}^{-1} \text{s}^{-1}$), f_c is the cloud volume fraction, and F_{aq} is the fraction of the chemical species that is in the aqueous phase (Table 4). The parameter F_{aq} was obtained assuming Henry's law of equilibrium for gases and for SO_2 subsequent dissociation in HSO_3^- and SO_3^{2-} . It is set to 0.7 and 0.5 for sulphate mass concentrations for accumulation and Aitken modes, respectively. This reflects the fact that a fraction of sulphate aerosols can be interstitial in clouds as shown by number of measurements (Boucher and Lohmann, 1995). In view of measurements given in Pruppacher and Klett (1997), F_{aq} is taken to be smaller

Tropospheric distribution of sulphate aerosol

S. Verma et al.

Title Page

Abstract

Introduction

Conclusions

References

Tables

Figures

◀

▶

◀

▶

Back

Close

Full Screen / Esc

Print Version

Interactive Discussion

Tropospheric distribution of sulphate aerosol

S. Verma et al.

Title Page

Abstract

Introduction

Conclusions

References

Tables

Figures

◀

▶

◀

▶

Back

Close

Full Screen / Esc

Print Version

Interactive Discussion

EGU

for sulphate number concentration at 0.5 and 0.3 for accumulation and Aitken modes, respectively. The parameter ϕ at model level k was computed from the precipitation flux (P_r , stratiform or convective, in $\text{kg m}^{-2} \text{s}^{-1}$) and a prescribed liquid water content ($q_l=0.5$ and 1.0 g kg^{-1} for stratiform and convective clouds, respectively)

$$\phi_k = \frac{P_{r,k} - P_{r,k+1}}{\rho_{air,k} z_k q_l} \quad (5)$$

where ρ_{air} is the air density (kg m^{-3}), z_k is the thickness of layer k . It was not distinguished between liquid and ice precipitation as far as in-cloud scavenging is concerned. Below-cloud scavenging is considered for aerosols only. Integrating over the population of raindrops for the volume space that is swept by a raindrop during its fallout, gives the expression for the scavenging rate, S_{bc} (s^{-1})

$$S_{bc} = \frac{3 P_r \eta}{4 R_r \rho_{water}} \quad (6)$$

where R_r is an average raindrop radius (set to 1 mm), ρ_{water} is the density of water and η is the efficiency with which aerosols are collected by raindrops. Based on measurement compiled by Pruppacher and Klett (1997), values of parameter η for raindrops and snowflakes were selected as 0.001 and 0.01, respectively. Three dimensional precipitation fluxes are computed in the GCM, obviating the need to assume vertical profiles of precipitation. Scavenged gases and aerosols are released back to the environment upon evaporation of raindrops. The release of a gas at a level k is equal to its amount scavenged at higher levels, multiplied by the fraction of precipitation, which is evaporated. For the release of aerosols, a factor of 0.5 was applied to account for the fact that raindrop can shrink without evaporating totally. In the event of total evaporation of the precipitation flux, whole of the aerosols are released to the atmosphere as well.

2.4. Convective transport

The mass fluxes, simulated by the [Tiedtke \(1989\)](#) scheme, are used to parameterise convective transport of gases and aerosols. Vertical transport of trace species is incorporated in updrafts and downdrafts, accounting for entrainment and detrainment.

5 Convective transport is performed after the wet scavenging calculation, in order to avoid upward transport of material that is scavenged by precipitation. Convective transport is applied in a bulk manner without distinguishing between the interstitial and the dissolved fraction of trace gases and aerosols. Moreover, a fraction (C_v) of aerosol mass and number, as well as soluble gases, which are detrained to the environment is
10 scavenged (Table 4). This additional term accounts for the processing of air from the environment in convective updrafts ([Crutzen and Lawrence, 2000](#); [Reddy et al., 2004](#)). Note that C_v is taken larger for the accumulation mode as compared to the Aitken mode, and larger for aerosol number as compared to aerosol mass concentration.

2.5. Aerosol optical and radiative properties

15 Mie theory is employed to compute the optical properties with prescribed size distribution and refractive indices. Optical properties are computed over the entire shortwave spectrum (0.25–4.0 μm) at 24 wavelengths and grouped into the two model wavebands as weighted averages with a typical spectral distribution of the incoming solar radiation flux at the surface. Depending upon their chemical nature aerosol take up water and
20 grow in size with relative humidity (RH). Thus RH affects both the particle size and density of sulphate aerosols. In the radiative code of LMDZ, the shortwave spectrum is divided into two intervals: 0.25–0.68 and 0.68–4.0 μm . The model accounts for the diurnal cycle of solar radiation and allows fractional cloudiness to form in a grid box. The shortwave radiative fluxes at the top of atmosphere (TOA) and at the surface
25 are computed every two hours with or without the presence of clouds and aerosols. The clear-sky and all-sky radiative forcing can then be estimated as the differences in shortwave radiative fluxes with and without aerosols. The cloud droplet number con-

Tropospheric distribution of sulphate aerosol

S. Verma et al.

Title Page

Abstract

Introduction

Conclusions

References

Tables

Figures

◀

▶

◀

▶

Back

Close

Full Screen / Esc

Print Version

Interactive Discussion

centration (N_d) is determined using the relation of Jones et al. (1994)

$$N_d = \max\{3.75 \times 10^8(1 - \exp[-2.5 \times 10^{-9}A]), N_{min}\} \quad (7)$$

where A is the sulphate number concentration in the accumulation mode and N_{min} has been set to a value $5 \times 10^6 \text{ m}^{-3}$. The droplet number N_d obtained from Eq. (7) is then used for calculating the effective cloud drop radius (r_e) in the model, which is further used to calculate the cloud optical thickness (τ) and cloud emissivity (ϵ) as

$$\tau = \frac{3W}{2\rho_{water}r_e}, \quad \epsilon = 1 - e^{-\kappa W} \quad (8)$$

The effective radius of cloud drop radius (r_e) is calculated from the radii of warm clouds and ice clouds. The absorption coefficient (κ) is set equal to $0.13 \text{ (m}^2 \text{ g}^{-1}\text{)}$ for all cloud types. W represent the cloud liquid path in Eq. (8). However, we do not show any result on the sulphate indirect effect in this study.

2.6. Emissions

Three SO_2 scenarios, which differ over India only, are used in the present study,

i) SCN-GEIA : emissions given for India in the Global Emission Inventory Activity (GEIA) inventory,

ii) SCN-RV : emissions of Reddy and Venkataraman (2002a,b) inventory (RV) for India,

iii) SCN-zero : emission from all over the world except India (i.e. emissions over India are set to zero). The global sulphur emissions in GEIA database include emissions from fossil fuels combustion and industrial processes. The biomass burning sulphur emissions are from Pham et al. (1995). A fixed 5% of sulphur from combustion sources is assumed to be emitted directly as sulphate mass in accumulation mode. The number concentration in the accumulation mode is not affected by these 5% emissions. The annual anthropogenic SO_2 emissions (man-made) from fossil fuel combustion and industrial activities are $66.31 \text{ Tg S yr}^{-1}$ globally with a contribution from India of 1.44 Tg

Title Page

Abstract

Introduction

Conclusions

References

Tables

Figures

◀

▶

◀

▶

Back

Close

Full Screen / Esc

Print Version

Interactive Discussion

S yr^{-1} which increases to $2.38 \text{ Tg S yr}^{-1}$ if RV inventory is used (Table 5). For biomass burning, the emission inventory for India is constructed using a spatially resolved data sets, which results in $0.33 \text{ Tg S yr}^{-1}$ as projection of SO_2 emission for the INDOEX period (1998–1999).

3. Results

3.1. Numerical simulations

The model simulations have been performed using 72 parallels between North and South Poles with 96 points on each parallel. There are 19 vertical levels and a basic time step of half an hour is used for the model physics and chemistry. For this study, the LMDZ was run in zoomed mode over the INDOEX study domain (25°S – 35°N , 50 – 100°E) with a uniform resolution of 1.25° in longitude and 1.25° in latitude at best around the zoom centre (60°E , 0°). The model initial state is prepared from 20 December 1998 ECMWF analysis and appropriate boundary conditions are set up, which are also specified from the ECMWF analyses of the IFP duration.

3.2. Model evaluation

3.2.1. The Kaashidhoo Climate Observatory

The simulated sulphate concentrations at the surface are compared with measured concentrations during INDOEX-IFP (February–March 1999) at Kaashidhoo Climate Observatory (KCO), Maldives in the Indian Ocean. KCO was established as a part of INDOEX in the island of Kaashidhoo (4.965°N , 73.466°E) about 500 km southwest of the southern tip of India, where the aerosol chemical, radiative, and microphysical properties were continuously measured since February 1998. The observatory serves as a key platform in the Arabian Sea. The aerosol characteristics observed at this loca-

Title Page

Abstract

Introduction

Conclusions

References

Tables

Figures

◀

▶

◀

▶

Back

Close

Full Screen / Esc

Print Version

Interactive Discussion

tion, from December to March, include both aerosols transported from the continents to the ocean and naturally produced at the ocean surface. The concentrations and properties of aerosols depend on the prevailing meteorological conditions. During the winter monsoon, the air mass over KCO mostly (about 90% of the time) originates from India and South Asia (Krishnamurthy et al., 1998).

3.2.2. Sulphate mass concentration and AOD at KCO

Here we compare the simulated sulphate concentration with corresponding measured concentration at KCO during INDOEX-IFP (Fig. 2). The emission inventory developed by Reddy and Venkataraman (RV) gives a better estimate of measured concentrations. Modelled surface sulphate concentrations agree with the measured values within a factor of 1–2. However, model simulation shows an increase in concentration in the month of February with RV inventory. This result is in general agreement with the meteorological conditions at KCO as most of the air mass during February originated from India in contrast to March when the air mass originated from East Asia (Verver et al., 2001) flows towards it. In contrast to surface concentrations, aerosol optical depth (AOD) is a measure of the aerosol entire column. The measured AOD from all aerosol species averaged over IFP at KCO was 0.37 ± 0.11 . Model simulated sulphate AOD at KCO ranged from 0.05 to 0.11 during the IFP period. The KCO aerosol measurements reveal that sulphate is responsible for 29% (Satheesh and Ramanathan, 2000; Satheesh et al., 1999) of the observed aerosol optical depth. Taking this fact into account, the model simulates the observed sulphate aerosol optical depth at KCO (Fig. 3) reasonably well.

3.2.3. Sulphate number concentration

Figure 4 illustrates the modelled and observed nucleation and total number concentrations along the cruise routes of the First Field Phase (FFP-98) and IFP-99. Kamra et al. (2003) observations show that more than 70% of the submicron aerosols advecting off

Title Page

Abstract

Introduction

Conclusions

References

Tables

Figures

◀

▶

◀

▶

Back

Close

Full Screen / Esc

Print Version

Interactive Discussion

**Tropospheric
distribution of
sulphate aerosol**S. Verma et al.

[Title Page](#)[Abstract](#)[Introduction](#)[Conclusions](#)[References](#)[Tables](#)[Figures](#)[◀](#)[▶](#)[◀](#)[▶](#)[Back](#)[Close](#)[Full Screen / Esc](#)[Print Version](#)[Interactive Discussion](#)

EGU

the continent consists of sulphate aerosols and for this reason we report 70% of their concentrations for the sake of comparing with the sulphate only modelled concentrations. The model is not expected to reproduce the variability in concentrations since the model meteorology is different from the actual one. However the model simulates the order of magnitude and the general north-south gradient in aerosol number concentrations. The fraction of total aerosols in the Aitken mode is quite different in 1999 as compared to 1998 and Kamra et al. (2003) do not have a clear explanation for this. The model simulates a fraction which is much more consistent than the values observed in 1998 as compared to 1999. The sources of uncertainty in simulating aerosol number concentrations are also reported in the literature, in particular, by Wilson et al. (2001) in a global model and Ackermann et al. (1998) in a mesoscale model using a similar approach and are worthy of further study.

3.3. Latitudinal variations

The latitudinal variation of sulphate number concentration and AOD in the Arabian Sea and Bay of Bengal for each month is discussed in this section. The latitudinal variations are obtained by separately averaging the variable values in the longitude ranges 60–80° E (Arabian Sea – Indian Ocean sector) and 80–100° E (Bay of Bengal – Indian Ocean sector).

3.3.1. Sulphate aerosol number concentration

Figure 5 represents latitudinal variations of sulphate aerosol number distributions during IFP 1999 over the Arabian Sea and Bay of Bengal sectors. One of the important feature captured by the model is that much lower concentrations are observed south of the Intertropical Convergence Zone (ITCZ). Latitudinal variations in the Arabian Sea sector of Aitken mode concentration (Fig. 5a) show a peak around 10–15° N region with a value of 8×10^3 particles cm^{-3} while in the Bay of Bengal sector the peak occurs around 25–30° N region with a maximum of 6.5×10^3 particles cm^{-3} , which decreases

**Tropospheric
distribution of
sulphate aerosol**

S. Verma et al.

Title Page

Abstract

Introduction

Conclusions

References

Tables

Figures

◀

▶

◀

▶

Back

Close

Full Screen / Esc

Print Version

Interactive Discussion

EGU

to the order of about 3×10^3 particles cm^{-3} upon reaching 5°S . This result is consistent with the finding of Lelieveld et al. (2001) who also report a drastic decrease in sulphate aerosols on crossing the ITCZ from north to south. The latitudinal variations of the accumulation mode concentration (Fig. 5b) show a larger magnitude over the Arabian Sea sector than the Bay of Bengal sector with elevated values in the interval $10\text{--}25^\circ\text{N}$. This indicates a strong influence of continental aerosols in the marine boundary layer over the Arabian Sea. The model predicts large aerosol concentrations ranging between 10^2 and 10^3 particles cm^{-3} over the North Indian Ocean during IFP and the contribution of Aitken mode concentration along north of ITCZ is significantly higher than that of the accumulation mode. These results generally agree with those of Lelieveld et al. (2001) and Kamra et al. (2003) who showed that the large number concentration during the IFP mostly consists of particles in the Aitken mode.

An observation on the number concentration and mass in the two modes is interesting. It may be noted that the number concentration in the Aitken mode over the Arabian sea reaches a peak value of 8×10^3 particles cm^{-3} with the corresponding mass of $0.6 \mu\text{g m}^{-3}$. On the contrary the number concentration in the accumulation mode reaches a maximum value of 1800 particles cm^{-3} and the corresponding mass there is about $4.6 \mu\text{g m}^{-3}$. This result is consistent with other studies, which have mentioned that most of the sulphate mass resides in the accumulation mode (Binkowski and Roselle, 2003).

3.3.2. Sulphate AOD

Figure 6 shows the latitudinal variations of aerosol optical depth during January, February and March 1999. The AOD is significantly larger in the Northern Hemisphere compared to the Southern Hemisphere during all three months, with maximum AOD near the continents. The latitudinal variation of sulphate AOD over the Arabian Sea sector (Fig. 6a) with Reddy and Venkataraman (RV) inventory shows a highest value (0.12) at

**Tropospheric
distribution of
sulphate aerosol**

S. Verma et al.

Title Page

Abstract

Introduction

Conclusions

References

Tables

Figures

◀

▶

◀

▶

Back

Close

Full Screen / Esc

Print Version

Interactive Discussion

EGU

around 25° N. A secondary peak is also observed at 10° N during the months of February and March. While in GEIA (Fig. 6c), latitudinal sulphate aerosol AOD is larger over (10–15° N), minimum in ITCZ and noticeably rises over the southern Indian Ocean (0–5° S) which then decreases linearly further southwards. The highest AOD is observed in the month of February with a value of 0.08 close to Arabia and the west coast of India. The plume extends from 15° N to 5° S in the month of January and March with highest values of 0.06 and 0.08, respectively. Over the Bay of Bengal sector (Fig. 6b) AOD is generally comparable to that over the Arabian Sea with superior values during January. For all three months, a plume lies in the region 20–25° N while another plume is also visible at 0–5° S region. The general features revealed by Fig. 6 are as follows: (i) the results show a southward migration of the AOD minimum in consonance with the migration of the ITCZ; (ii) there is a visible rise in sulphate AOD in the Arabian Sea sector over 0–10° S region with the Indian inventory (RV) suggesting the role of Indian emissions in these concentrations; (iii) the AOD in the Northern Hemisphere is larger than that of Southern Hemisphere by about 30–50%. These patterns derived from model-simulated values are mostly confirmed by satellite observed patterns especially the maxima over 10–25° N regions (Chowdhury et al., 2001; Quinn et al., 2002; Reddy et al., 2004).

3.4. Regional distribution for INDOEX-IFP

The equatorial Indian Ocean region provides a unique opportunity to observe anthropogenic sulphate effects. From January to April, the predominant circulation in this region consists of a low-level flow from the northeast (Krishnamurthy et al., 1998). This NE monsoon (Asian winter monsoon) should facilitate the formation and transport of new sulphate particles to oceanic regions far away from urban centres. The above feature is very crucial as atmospheric circulation and aerosol lifetimes are the dominant factors controlling both spatial distribution and transport of aerosols that could be evaluated through a chemistry-transport model.

3.4.1. SO₂ concentration

The model simulated spatial distribution of SO₂ concentration over surface and column burden are shown (Fig. 7) over the INDOEX domain averaged for January, February and March 1999. The largest values at surface are found over southeastern China, western and eastern parts of India (8–10 μg m⁻³). Concentrations of SO₂ over ocean are low indicating the short chemical lifetime.

3.4.2. Sulphate mass and number concentrations

The average surface concentrations (Fig. 8a) over SE China (>5 μg SO₄²⁻m⁻³) are higher than over India (3–4 μg SO₄²⁻m⁻³) with elevated values 4–5 μg m⁻³ over north-east India. The plume extends over the Arabian Sea (2–3 μg SO₄²⁻m⁻³), the Bay of Bengal (1–3 μg SO₄²⁻m⁻³) and the Northern Indian Ocean (0.5–2 μg SO₄²⁻m⁻³) indicating advection of sulphate from continents to ocean. The sulphate column burden (Fig. 8b) show a high over south and east India (8–10 mg SO₄²⁻m⁻²). The average vertical profile of sulphate aerosol loading (Fig. 9) also looks reasonable with constant concentration up to a level of about 900 hPa and then a substantial decrease by at least a factor of 2 at about 3 km (700 hPa). Notably, the observations reported by Rasch et al. (2001) also support the simulated average sulphate concentration for the entire INDOEX region during IFP and are consistent with earlier modelling studies. The Aitken mode average concentration (4×10³–6×10³ particles cm⁻³) over India (Fig. 10) is more as compared to the accumulation mode (1×10³–2×10³ particles cm⁻³) with a maximum over western India (3×10³–4×10³ particles cm⁻³) extending to the Arabian Sea region. Since the precursor gases for the formation of these sub-micron particles comes mostly from the continents, the model reveals SE China and Indian region as important contributors to anthropogenic sulphate aerosol production. The observed decrease in the concentration of particles in the accumulation mode from north to south is due to the removal of these particles by dry and wet deposition (Kamra et al., 2003).

Title Page

Abstract

Introduction

Conclusions

References

Tables

Figures

◀

▶

◀

▶

Back

Close

Full Screen / Esc

Print Version

Interactive Discussion

**Tropospheric
distribution of
sulphate aerosol**

S. Verma et al.

Title Page

Abstract

Introduction

Conclusions

References

Tables

Figures

◀

▶

◀

▶

Back

Close

Full Screen / Esc

Print Version

Interactive Discussion

EGU

Wind vectors at the surface (Fig. 11a) show strong outflows from north and east India into the Arabian Sea and Northern Indian Ocean. These strong flows explain the plausible cause of advection of SO₂ and sulphate from continents and contribute to sulphate column burden over oceanic regions.

5 3.4.3. Sulphate AOD and its radiative properties

In Fig. 12a, the geographical distribution of the sulphate aerosol optical depth during the INDOEX period is presented. The largest values in AOD lie over SE China where the anthropogenic source of sulphur is very intense. An area of large AOD (0.1–0.14) and radiative forcing at top of atmosphere (-1.25 to -2.0 m⁻²) is observed (Fig. 12b) from this region covering India; AOD over northern India (0.04–0.1) extends deep into the Arabian Sea and the Indian Ocean region (down to 10° S). Higher AOD values are also noted over southeastern part of India with a maximum reaching 0.12. From coast to the central Bay of Bengal lower values of AOD occur, where aerosol transport both from India and South-East Asia, is insignificant and reflects the impact of anticyclonic circulation near South India (Rajeev et al., 2000), which does not allow the offshore flow from eastern India to penetrate deep into the Bay of Bengal. Smaller magnitude of radiative forcing (<0.75 W m⁻²) and AOD (<0.04) are present south to 5° S, near the ITCZ (Quinn et al., 2002).

3.5. Indian source contribution to sulphate burden

The Indian emissions are carried deep down into the Arabian Sea sector and to the coastal Bay of Bengal region. Thus the air from India contributes more strongly to Arabian Sea and to the near coastal region of Bay of Bengal. The large aerosol plume off the southwest coast is particularly noticeable (Fig. 13). There is a visible Asian plume entering at about 15–25° N, 90° E, contributing significantly to sulphate burden. Atmospheric circulation and trajectory analysis for INDOEX region has shown large southwestward transport of air from peninsular India at lower tropospheric levels. As

a consequence, large amount of sulphate off the west coast of India has been transported over to oceanic regions. Over the Bay of Bengal region there is considerable transport of air from southeast Asia due to prevailing easterly and northeasterly winds (Krishnamurthy et al., 1998; Rajeev et al., 2000; Rasch et al., 2001).

4. Conclusions

In this study, a newly developed interactive sulphur chemistry (gas-phase and aqueous phase) with a comprehensive aerosol module is implemented in Laboratoire de Météorologie Dynamique General Circulation model (LMD-GCM). The model simulates the sulphate AOD, mass and number concentration to reasonably acceptable levels in the entire INDOEX region for the IFP. At Kaashidhoo, the model simulated sulphate values agree with observations within a factor of 2–3. In general, the plume of sulphate mass, number concentration and aerosol optical depth in the Northern Hemisphere is larger than that of Southern Hemisphere by ~30–50%, which follows the migration of ITCZ with a minimum centred around this region.

In conclusion, Indian emissions however are not the sole cause for the high sulphate and AOD concentrations over the Indian Ocean. The Indian contribution is more than 60% over India and 30–50% over the Arabian Sea. Over the Bay of Bengal in addition to Indian emissions, aerosols transported from the East Asia also contribute significantly to sulphate burden. Transport of aerosol by northwesterly winds from Arabia and northeasterly winds from the Indian subcontinent are the major sources of higher concentrations over the Arabian Sea; whereas over the Bay of Bengal, the transport is mainly from Southeast Asia. It is finally remarked that the results reported have been produced for single aerosol type (sulphate) and considers the contribution from total emission (anthropogenic as well as natural).

Acknowledgements. This work was initiated at LMD with the encouragement from R. Sadourny (LMD), C. Basdevant (LMD), K. Laval (LMD), T. N. Krishnamurti (FSU, Tallahassee) and V. Ramanathan (SIO, La Jolla), when one of us (OPS) was a Visiting Professor to Ecole Nor-

**Tropospheric
distribution of
sulphate aerosol**

S. Verma et al.

Title Page

Abstract

Introduction

Conclusions

References

Tables

Figures

◀

▶

◀

▶

Back

Close

Full Screen / Esc

Print Version

Interactive Discussion

male Supérieure (ENS) with the financial support of Ministère de l'Éducation Nationale, de l'Enseignement Supérieur et de la Recherche, Government of France. He also wishes to thank S. M. Kreidenweis (CSU, Fort Collins) for her valuable help in the initial stages of the aerosol module implementation. This work was supported by the Indo-French Centre for the Promotion of Advanced Research/Centre Franco-Indien Pour la Recherche Avancée under project 1911-2. Also for a part of development work in this study the computational support was provided by the Institut du Développement et des Ressources en Informatique Scientifique (IDRIS) of CNRS (France) under project 031167.

References

- Ackermann, I. J., Hass, H., Memmesheimer, M., Ebel, A., Binkowski, F. S., and Shankar, U.: Modal aerosol dynamics for Europe: Development and first applications, *Atmos. Envir.*, 32 (17), 2981–2999, 1998. [408](#)
- Atkinson, R., Baulch, D. L., Cox, R. A., Hampson, R. F., Kerre Jr., J. A., and Troe, J.: Evaluated kinetic and photochemical data for atmospheric chemistry: Supplement III, *J. Phys. Chem. Ref. Data*, 18, 881–1097, 1989. [399](#), [419](#)
- Binkowski, F. S. and Roselle, S. J.: Models-3 community multiscale air quality (CMAQ) model aerosol component 1. model description, *J. Geophys. Res.*, 108 (D6), 4183, doi:10.1029/2001JD001409, 2003. [401](#), [409](#)
- Binkowski, F. S. and Shankar, U.: The regional particulate matter model: Part 1, model description and preliminary results, *J. Geophys. Res.*, 100, 26 191–26 209, 1995. [401](#)
- Boer, G. J.: Some results from an intercomparison of the climates simulated by 14 atmospheric general circulation models, *J. Geophys. Res.*, 97, 12 771–12 786, 1992. [398](#)
- Boucher, O. and Lohmann, U.: The sulfate-CCN-cloud albedo effect: a sensitivity study using two general circulation models, *Tellus* 47B, 281–300, 1995. [398](#), [402](#)
- Boucher, O., Pham, M., and Sadourny, R.: General circulation model simulation of Indian summer monsoon with increasing levels of sulphate aerosols, *Ann. Geophys.*, 16, 346–352, 1998. [398](#)
- Boucher, O., Pham, M., and Venkataraman, C.: Simulation of the atmospheric sulphur cycle in the Laboratoire de Météorologie Dynamique general circulation model: Model description,

Tropospheric distribution of sulphate aerosol

S. Verma et al.

Title Page

Abstract

Introduction

Conclusions

References

Tables

Figures

◀

▶

◀

▶

Back

Close

Full Screen / Esc

Print Version

Interactive Discussion

- 30 model evaluation, and global and European budgets, Note scientifique de l'IPSL n°23, 2002.
[398](#), [399](#), [400](#)
- Cess, R. D., Potter, G. L., Blanchet, J. P., Boer, G. J., Ghan, S. J., Kiehl, J. T., Le Treut, H., Li, Z.-X., Liang, X.-Z., Mitchell, J. F. B., Morcrette, J.-J., Randall, D. A., Riches, M. R., Roeckner, E., Schlese, U., Slingo, A., Taylor, K. E., Washington, W. M., Wetherald, R. T., and Yagai, I.:
5 Interpretation of cloud-climate feedback as produced by 14 atmospheric general circulation models, *Science*, 245, 513–516, 1989. [398](#)
- Charlson, R. J., Schwartz, S. E., Hales J. M., Cess, R. D., Coakley, J. A., Hansen, J. E., and Hotmann, D. J.: Climate forcing by anthropogenic aerosols, *Science*, 255, 423–430, 1992.
[396](#)
- 10 Chatfield, R. B. and Crutzen, P. J.: Are there interactions of iodine and sulfur species in marine air photochemistry?, *J. Geophys. Res.*, 95, 22 319–22 341, 1990. [399](#), [419](#)
- Chen, J.-P. and Crutzen, P. J.: Solute effect on the evaporation of ice particles, *J. Geophys. Res.*, 99, 18 847–18 859, 1994. [399](#), [400](#), [419](#), [420](#)
- Chowdhury, Z., Hughes, L. S., and Salmon, L. G.: Atmospheric particle size an composition measurements to support light extinction calculation over the Indian Ocean, *J. Geophys. Res.*, 106, 28 597–28 605, 2001. [410](#)
- 15 Crutzen, P. J. and Lawrence, M. G.: The impact of precipitation scavenging on the transport of trace gases, *J. Atmos. Chem.*, 37, 81–112, 2000. [404](#)
- Giorgi, F. and Chameides, W. L.: Rainout lifetimes of highly soluble aerosols and gases as inferred from simulations with a general circulation model, *J. Geophys. Res.*, 91, 14 367–14 376, 1986. [402](#)
- 20 Harrington, D. Y. and Kreidenweis, S. M.: Simulations of sulfate aerosol dynamics: Part I model description, *Atmos. Envir.*, 32, 1691–1700, 1998a. [401](#)
- Harrington, D. Y. and Kreidenweis, S. M.: Simulations of sulfate aerosol dynamics: Part II model intercomparison, *Atmos. Envir.*, 1701–1709, 1998b. [401](#)
- 25 Hauglustaine, D. A., Hourdin, F., Jourdain, L., Filiberti, M.-A., Walters, S., Lamarque, J.-F., and Holland, E. A.: Interactive chemistry in the Laboratoire de Météorologie Dynamique general circulation model: description and background tropospheric chemistry evaluation, *J. Geophys. Res.*, 109, D04314, doi:10.1029/2003JD003957, 2004. [399](#)
- 30 Hegg, D. A. and Hobbs, P. V.: Cloud water chemistry and the production of sulfates in clouds, *Atmos. Envir.*, 15, 1597–1604, 1981. [400](#)
- Hesstvedt, E., Hov, Ö., and Isaksen, I. S. A.: Quasi-steady-state-approximation in air pollution

**Tropospheric
distribution of
sulphate aerosol**S. Verma et al.

[Title Page](#)[Abstract](#)[Introduction](#)[Conclusions](#)[References](#)[Tables](#)[Figures](#)[◀](#)[▶](#)[◀](#)[▶](#)[Back](#)[Close](#)[Full Screen / Esc](#)[Print Version](#)[Interactive Discussion](#)

**Tropospheric
distribution of
sulphate aerosol**

S. Verma et al.

[Title Page](#)[Abstract](#)[Introduction](#)[Conclusions](#)[References](#)[Tables](#)[Figures](#)[◀](#)[▶](#)[◀](#)[▶](#)[Back](#)[Close](#)[Full Screen / Esc](#)[Print Version](#)[Interactive Discussion](#)

EGU

modelling: comparison of two numerical schemes for oxidant prediction, *Int. J. Chem. Kinet.*, 10, 971–994, 1978. [400](#)

Hourdin, F. and Armengaud, A.: On the use of finite volume methods for atmospheric advection of trace species: I. Test of various formulations in a general circulation model, *Mon. Wea. Rev.*, 127, 822–837, 1999. [399](#)

5 Jones, A., Roberts, D. L., Woodage, M. J., and Johnson, C. E.: Indirect sulphate aerosol forcing in a climate model with an interactive sulphur cycle, *J. Geophys. Res.*, 106, 20 293–20 310, 2001. [405](#)

Kamra, A. K., Murugavel, P., and Pawar, S. D.: Measured size distributions of aerosols over the Indian Ocean during INDOEX, *J. Geophys. Res.*, 108 (D3), 8000, doi:10.1029/2002JD002200, 2003. [407](#), [409](#), [411](#), [427](#)

10 Kiehl, J. T. and Briegleb, B. P.: The relative role of sulphate aerosols and greenhouse gases in climate forcing, *Science*, 260, 311–314, 1993. [396](#)

Krishnamurthy, T. N., Jha, B., Prospero, J. M., Jayaraman, A., and Ramanathan, V.: Aerosol and pollutant transport and their impact on radiative forcing over tropical Indian Ocean during January–February 1996 pre-INDOEX cruise, *Tellus B*, 50, 521–542, 1998. [397](#), [407](#), [410](#), [413](#)

Kulmala, M., Laaksonen, A., and Pirjola, L.: Parameterization for sulphuric acid/water nucleation rates, *J. Geophys. Res.*, 103, 8301–8307, 1998. [401](#)

15 Lawrence, M. G., Crutzen, P. J., Rasch, P. J., Eaton, B. E., and Mahowald, M.: A model for studies of tropospheric chemistry: Description, global distributions, and evaluation, *J. Geophys. Res.*, 104, 26 245–26 277, 1999. [399](#), [419](#)

Lelieveld, J., Crutzen, P. J., Ramanathan, V., et al.: The Indian Ocean Experiment: Widespread air pollution from south and southeast Asia, *Science*, 291, 1031–1035, 2001. [409](#)

20 Le Treut, H., Li, Z. X., and Forichon, M.: Sensitivity study of LMD GCM to greenhouse forcing associated with two different cloud water parametrization, *J. Climate*, 7, 1827–1841, 1994. [398](#), [399](#)

Li, Z. X.: Ensemble atmospheric GCM simulation of climate interannual variability from 1979 to 1994, *J. Climate*, 12, 986–1001, 1999. [399](#)

25 Lott, F.: Alleviation of stationary bias in a GCM through a mountain drag parametrization scheme and a simple representation of mountain lift forces, *Mon. Wea. Rev.*, 127, 788–801, 1999. [399](#)

30 Ohta, S., Okita, T., and Kato, C.: A numerical model of acidification of cloud water, *J. Meteor.*

**Tropospheric
distribution of
sulphate aerosol**

S. Verma et al.

[Title Page](#)[Abstract](#)[Introduction](#)[Conclusions](#)[References](#)[Tables](#)[Figures](#)[◀](#)[▶](#)[◀](#)[▶](#)[Back](#)[Close](#)[Full Screen / Esc](#)[Print Version](#)[Interactive Discussion](#)

EGU

Soc. Japan, 6, 59, 1981. [400](#)

Pham, M., Muller, J.-F., Brasseur, G., Granier, C., and Mégie, G.: A 3-D model study of the global sulphur cycle: Contributions of anthropogenic and biogenic sources, *Atmos. Envir.*, 30, 1815–1822, 1995. [405](#)

Pruppacher, H. R. and Klett, J. D.: *Microphysics of clouds and precipitation*, second revised and enlarged edition with an introduction to cloud chemistry and cloud electricity, Kluwer Academic Publishers, Boston, 954, 1997. [402](#), [403](#)

Quinn, P. K., Coffman, D. J., Bates, T. S., Miller, T. L., Johnson, J. E., Welton, E. J., Neususs, C., Miller, M., and Sheridan, P. J.: Aerosol optical properties during INDOEX-1999: Means, variability, and controlling factors, *J. Geophys. Res.*, 107(D19), 8020, doi:10.1029/2000JD000037, 2002. [410](#), [412](#)

Rajeev, K., Ramanathan, V., and Maywerk, J.: Regional aerosol distribution and its long range transport over the Indian Ocean, *J. Geophys. Res.*, 105, 2029–2043, 2000. [397](#), [412](#), [413](#)

Ramanathan, V., Crutzen, P. J., Lelieveld, J., et al.: The Indian Ocean Experiment: An integrated analysis of the climate forcing and effects of the great Indo-Asian haze, *J. Geophys. Res.*, 106, 28 371–28 398, 2001. [397](#)

Rasch, P. J., Collins, W. D., and Eaton, B. E.: Understanding the Indian Ocean experiment aerosol distribution with an aerosol assimilation, *J. Geophys. Res.*, 106, 7337–7356, 2001. [397](#), [411](#), [413](#)

Reddy, M. S. and Venkataraman, C.: Inventory of aerosol and sulphur dioxide emissions from India: I – Biomass combustion, *Atmos. Envir.*, 36, 677–697, 2002a. [397](#), [405](#)

Reddy, M. S. and Venkataraman, C.: Inventory of aerosol and sulphur dioxide emissions from India: II – Biomass combustion, *Atmos. Envir.*, 36, 699–712, 2002b. [397](#), [405](#)

Reddy, M. S., Boucher, O., Venkataraman, C., Verma, S., Léon, J.-F., Bellouin, N., and Pham, M.: GCM estimates of aerosol transport and radiative forcing during INDOEX, *J. Geophys. Res.*, 109(D16), D16205, doi:10.1029/2004JD004557, 2004. [404](#), [410](#)

Sadourny, R. and Laval, K.: January and July performances of LMD general circulation model, *New perspectives in Climate Modelling*, edited by: Berger, A., Elsevier, 173–198, 1984. [398](#), [399](#)

Satheesh, S. K. and Ramanathan, V.: Large differences in tropical aerosol forcing at the top of the atmosphere and Earth's surface, *Nature*, 405, 60–63, 2000. [397](#), [407](#)

Satheesh, S. K., Ramanathan, V., Jones, X., Lobert, J. M., Podgorny, I. H., Prospero, J. M., Holben, B. N., and Loeb, N. G.: A model for the natural and anthropogenic aerosols over the

tropical Indian Ocean derived from Indian Ocean Experiment data, J. Geophys. Res., 104, 27 421–27 440, 1999. [407](#)

Sharma, O. P., Le Treut, H., Sèze, G., Fairhead, L., and Sadourny, R.: Interannual variations of summer monsoons: Sensitivity to cloud radiative forcing, J. Climate, 11, 1883–1905, 1998. [398](#)

5 Snider, J. R. and Vali, G.: Sulphur dioxide oxidation in winter orographic clouds, J. Geophys. Res., 99, 18 713–18 733, 1994. [400](#)

Tiedtke, M.: A comprehensive mass flux scheme for cumulus parameterization in large scale models, Quart. J. Roy. Meteor. Soc., 117, 1779–1800, 1989. [404](#)

10 UNEP and C⁴: The Asian brown cloud: climate and other environmental impacts UNEP, Nairobi, 2002. [397](#)

Verver, G. H. L., Sikka, D. R., Lobert, J. M., Stossmeister, G., and Zachariasse, M.: Overview of the meteorological conditions and atmospheric transport during INDOEX 1999, J. Geophys. Res., 106, 28 399–28 414, 2001. [397](#), [407](#)

605 Walcek, C. J. and Taylor, R.: A theoretical method for computing vertical distribution of acidity and sulfate production with cumulus clouds, J. Atmos. Sci., 43, 339–355, 1986. [400](#)

Wilson, J., Curvelier, C., and Raes, F.: A modeling study of global mixed aerosol fields, J. Geophys. Res., 106, 34 081–34 108, 2001. [408](#)

**Tropospheric
distribution of
sulphate aerosol**

S. Verma et al.

Title Page

Abstract

Introduction

Conclusions

References

Tables

Figures

◀

▶

◀

▶

Back

Close

Full Screen / Esc

Print Version

Interactive Discussion

Table 1. Rate reactions for gas-phase chemistry.

S.No.	Reaction	Rate
1.	$O_3 + hv \rightarrow O(^1D) + O_2$	$J_1 = 1.5 \times 10^{-5}$
2.	$O(^1D) + O_2 (+M) \rightarrow O_3 (+M)$	$k_2 = 3.2 \times 10^{-11} \exp(67/T)$
3.	$O(^1D) + H_2O \rightarrow 2 OH$	$k_3 = 2.2 \times 10^{-10}$
4.	$CH_4 + OH + O_2 \rightarrow CH_3O_2 + H_2O$	$k_4 = 3.9 \times 10^{-12} \exp(-1885/T)$
5.	$CH_3O_2 + NO \rightarrow CH_3O + NO_2$	$k_5 = 4.2 \times 10^{-12} \exp(180/T)$
6.	$CH_3O + O_2 \rightarrow CH_2O + HO_2$	$k_6 = 7.2 \times 10^{-14} \exp(-1080/T)$
7a.	$CH_2O + hv \rightarrow CO + H_2$	$k_{7a} = 70\% \text{ of } k_6$
7b.	$CH_2O + hv + 2O_2 \rightarrow CO + 2HO_2$	$k_{7b} = 30\% \text{ of } k_6$
8.	$CO + HO + O_2 \rightarrow CO_2 + HO_2$	$k_8 = 1.5 \times 10^{-13} (1 + 0.6P)$
9.	$HO_2 + NO \rightarrow OH + NO_2$	$k_9 = 3.7 \times 10^{-12} \exp(240/T)$
10.	$HO_2 + O_3 \rightarrow OH + 2O_2$	$k_{10} = 1.4 \times 10^{-14} \exp(-600/T)$
11.	$HO_2 + HO_2 \rightarrow H_2O_2 + O_2$	$k_{11} = 2.2 \times 10^{-13} \exp(600/T) + 1.9e-33 \exp(980/T) M$
12.	$H_2O_2 + hv \rightarrow 2HO$	$J_{12} = 5 \times 10^{-6}$
13.	$H_2O_2 + OH \rightarrow HO_2 + H_2O$	$k_{13} = 2.9 \times 10^{-12} \exp(-160/T)$
14.	$HO + SO_2 \rightarrow H_2SO_4 + HO_2$	$k_{14} = 2. \times 10^{-12}$
15.	$OH + NO_2 + M \rightarrow HNO_3 + M$	$k_{15} = 6 \times 10^{-11}$
16.	$NO + O_3 \rightarrow NO_2 + O_2$	$k_{16} = 1.8 \times 10^{-12} \exp(-1370/T)$
17.	$NO_2 + hv \rightarrow NO + O$	$J_{17} = 7 \times 10^{-3}$
18.	$DMS + OH \rightarrow SO_2 + 2HCHO$	$k_{17} = 9.6 \times 10^{-12} \exp(-234/T)$
19.	$H_2S + OH \rightarrow SO_2 + HO_2$	$k_{18} = 1.9 \times 10^{-13} \exp(500/T)$
20.	$DMSO + OH \rightarrow 0.6SO_2 + 0.4MSA + 1.5HCHO$	$k_{19} = 5.8 \times 10^{-11}$
21.	$DMS + OH \rightarrow 0.6SO_2 + 0.4DMSO + 1.5HCHO$	$k_{20} = 3.04 \times 10^{-12} \exp(350/T) \alpha (1 + \alpha)$ where $\alpha = 1.15 \times 10^{-31} \exp(7460/T)$

J is given in s^{-1} ; k in $cm^3 \text{ molecule}^{-1} s^{-1}$; P is pressure in atm; T is in K; M represents N_2 or O_2 or another third molecule.

The reaction rates are from [Chen and Crutzen \(1994\)](#) and [Lawrence et al. \(1999\)](#) except reactions (18–21), which are from [Atkinson et al. \(1989\)](#) and [Chatfield and Crutzen \(1990\)](#).

Tropospheric distribution of sulphate aerosol

S. Verma et al.

Title Page

Abstract

Introduction

Conclusions

References

Tables

Figures

◀

▶

◀

▶

Back

Close

Full Screen / Esc

Print Version

Interactive Discussion

EGU

Title Page

Abstract

Introduction

Conclusions

References

Tables

Figures

◀

▶

◀

▶

Back

Close

Full Screen / Esc

Print Version

Interactive Discussion

EGU

Table 2. Rate reactions for aqueous-phase chemistry.

S.No.	Reaction	Rate
1.	$\text{H}_2\text{O} \leftrightarrow \text{H}^+ + \text{OH}^-$	$K_w = \exp(-9.731-6710/T)$
2.	$\text{CO}_2(\text{g}) \leftrightarrow \text{CO}_2 \cdot \text{H}_2\text{O}$	$H_2 = \exp(-11.50+2420/T)$
3.	$\text{CO}_2 \cdot \text{H}_2\text{O} \leftrightarrow \text{H}^+ + \text{HCO}_3^-$	$K_3 = \exp(-18.98-1000/T)$
4.	$\text{HCO}_3^- \leftrightarrow \text{H}^+ + \text{CO}_3^{2-}$	$K_4 = \exp(-17.86-1760/T)$
5.	$\text{SO}_2(\text{g}) \leftrightarrow \text{SO}_2 \cdot \text{H}_2\text{O}$	$H_5 = \exp(-10.26+3120/T)$
6.	$\text{SO}_2 \cdot \text{H}_2\text{O} \leftrightarrow \text{H}^+ + \text{HSO}_3^-$	$K_6 = \exp(-10.97+1960/T)$
7.	$\text{HSO}_3^- \leftrightarrow \text{H}^+ + \text{SO}_3^{2-}$	$K_7 = \exp(-21.56+1500/T)$
8.	$\text{H}_2\text{SO}_4(\text{g}) \leftrightarrow \text{H}_2\text{SO}_4 \cdot \text{H}_2\text{O}$	$H_8 = \exp(-25.73+17339/T)$
9.	$\text{H}_2\text{SO}_4 \cdot \text{H}_2\text{O} \leftrightarrow \text{H}^+ + \text{HSO}_4^-$	$K_9 = 1000$
10.	$\text{HSO}_4^- \leftrightarrow \text{H}^+ + \text{SO}_4^{2-}$	$K_{10} = \exp(-13.71+2720/T)$
11.	$\text{HNO}_3(\text{g}) \leftrightarrow \text{HNO}_3 \cdot \text{H}_2\text{O}$	$H_{11} = 2.1 \times 10^5$
12.	$\text{HNO}_3 \cdot \text{H}_2\text{O} \leftrightarrow \text{H}^+ + \text{HNO}_3^-$	$K_{12} = \exp(-26.46+8700/T)$
13.	$\text{NH}_3(\text{g}) \leftrightarrow \text{NH}_3 \cdot \text{H}_2\text{O}$	$H_{13} = \exp(-7.086+3400/T)$
14.	$\text{NH}_3 \cdot \text{H}_2\text{O} \leftrightarrow \text{OH}^- + \text{NH}_4^+$	$K_{14} = \exp(-9.444-450/T)$
15.	$\text{O}_3(\text{g}) \leftrightarrow \text{O}_3 \cdot \text{H}_2\text{O}$	$H_{15} = \exp(-12.20+2300/T)$
16.	$\text{H}_2\text{O}_2(\text{g}) \leftrightarrow \text{H}_2\text{O}_2 \cdot \text{H}_2\text{O}$	$H_{16} = \exp(-10.99+6620/T)$
17.	$\text{S(IV)} + \text{O}_3 \rightarrow \text{S(VI)} + \text{O}_2$	$J_{17a} = 2.4 \times 10^4$ $J_{17b} = \exp(31.37-5530/T)$ $J_{17c} = \exp(38.84-5280/T)$
18.	$\text{S(IV)} + \text{H}_2\text{O}_2 \rightarrow \text{S(VI)} + \text{H}_2\text{O}$	$J_{18} = \exp(34.33-4751/T)$

K_w is given in M^2 ; H is in M atm^{-1} ; J_{17} is in $\text{M}^{-1}\text{s}^{-1}$; J_{18} is in $\text{M}^{-2}\text{s}^{-1}$ and T is in Kelvin. Reactions rates are from [Chen and Crutzen \(1994\)](#). The rate expression and rate constants for S(IV) with O_3 and H_2O_2 (reactions 17 and 18) are given as: $d[\text{S(IV)}]_{aq}/dt = -\{J_{17a}[\text{SO}_2 \cdot \text{H}_2\text{O}] + J_{17b}[\text{HSO}_3^-] + J_{17c}[\text{SO}_3^{2-}]\} [\text{O}_3]_{aq}$;

$d[\text{S(IV)}]_{aq}/dt = -J_{18}[\text{H}^+][\text{HSO}_3^-][\text{H}_2\text{O}_2]_{aq}/(1+k[\text{H}^+])$, where $k = 13 \text{ M}^{-1}$

Tropospheric distribution of sulphate aerosol

S. Verma et al.

Title Page

Abstract

Introduction

Conclusions

References

Tables

Figures

◀

▶

◀

▶

Back

Close

Full Screen / Esc

Print Version

Interactive Discussion

EGU

Table 3. Dry deposition velocities v_d (cm s^{-1}).

Surface	DMS	H ₂ S	DMSO	MSA	SO ₂	NO _x	CO	O ₃	H ₂ O ₂	Sulphate Mass		Sulphate Number	
										Aitken	Accum.	Aitken	Accum.
Ocean	0.0	0.0	1.0	0.05	0.7	0.001	0.0	0.0	0.01	0.05	0.05	0.05	0.05
Land	0.0	0.0	0.0	0.20	0.20	0.01	0.04	0.0	0.01	0.20	0.20	0.20	0.20
Ice	0.0	0.0	0.0	0.20	0.20	0.0	0.0	0.0	0.01	0.20	0.20	0.20	0.20

Tropospheric distribution of sulphate aerosol

S. Verma et al.

Table 4. Wet deposition properties.

Parameter	C_v	F_{aq}
DMS	0.2	Henry's law
H ₂ S	0.2	Henry's law
DMSO	0.2	Henry's law
MSA	0.5	0.7
SO ₂	0.2	Henry's law
NO _x	0.0	Henry's law
CO	0.0	Henry's law
O ₃	0.2	Henry's law
H ₂ O ₂	0.2	Henry's law
Sulfate mass Aitken	0.3	0.5
Sulfate mass accum.	0.5	0.7
Sulfate number Aitken	0.2	0.3
Sulfate number accum.	0.4	0.5

F_{aq} : fraction in aqueous phase;

C_v : fraction of detrained species which
is scavenged during convective transport;

[Title Page](#)
[Abstract](#)
[Introduction](#)
[Conclusions](#)
[References](#)
[Tables](#)
[Figures](#)
[◀](#)
[▶](#)
[◀](#)
[▶](#)
[Back](#)
[Close](#)
[Full Screen / Esc](#)
[Print Version](#)
[Interactive Discussion](#)

EGU

**Tropospheric
distribution of
sulphate aerosol**

S. Verma et al.

Table 5. Global annual sulphur emissions in the model (Tg S yr^{-1}).

Source	Global Emission (GEIA)	Indian Emission (GEIA)	Indian Emission (RV)
Biomass Burning	3.39	0.24	0.33
Fossil-Fuel	66.31	1.44	2.38
Total	70.30	1.68	2.71

[Title Page](#)[Abstract](#)[Introduction](#)[Conclusions](#)[References](#)[Tables](#)[Figures](#)[⏪](#)[⏩](#)[◀](#)[▶](#)[Back](#)[Close](#)[Full Screen / Esc](#)[Print Version](#)[Interactive Discussion](#)

EGU

Tropospheric distribution of sulphate aerosol

S. Verma et al.

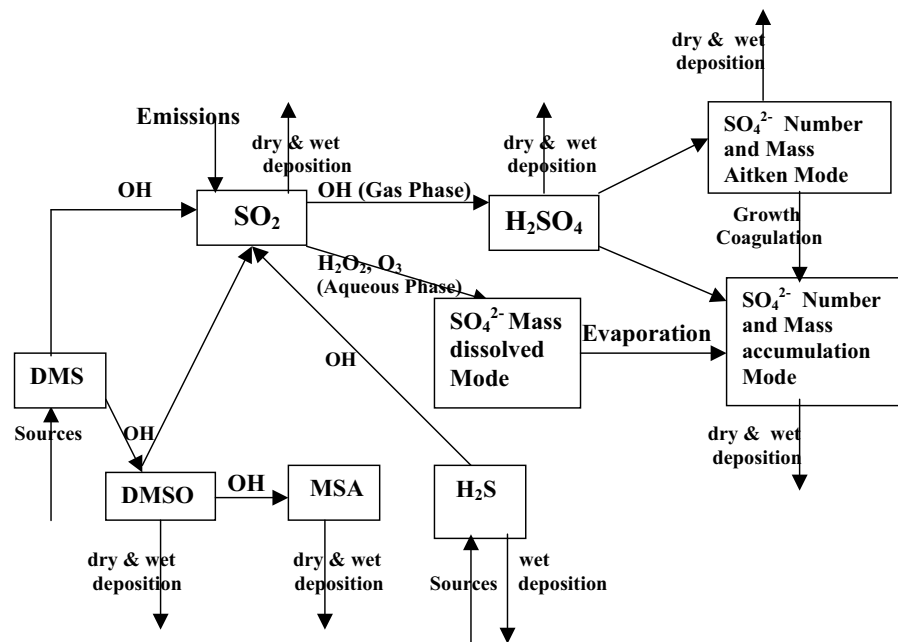


Fig. 1. The schematic representation of the sulphur module in the LMDZ.

[Title Page](#)
[Abstract](#)
[Introduction](#)
[Conclusions](#)
[References](#)
[Tables](#)
[Figures](#)
[◀](#)
[▶](#)
[◀](#)
[▶](#)
[Back](#)
[Close](#)
[Full Screen / Esc](#)
[Print Version](#)
[Interactive Discussion](#)

EGU

Tropospheric
distribution of
sulphate aerosol

S. Verma et al.

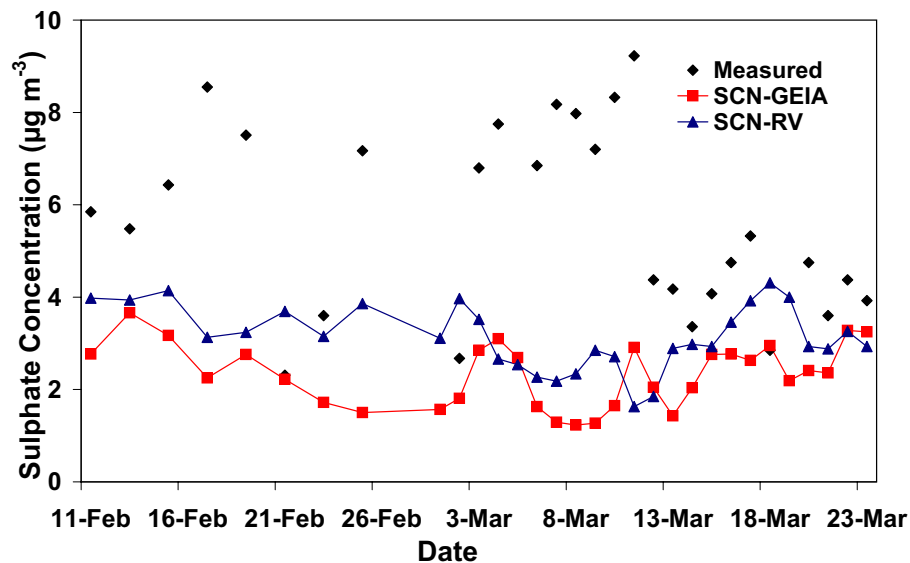


Fig. 2. Modelled (squares and triangles) and observed sulphate (diamonds) concentration at Kaashidhoo [73.46° E, 4.96° N] during INDOEX-IFP.

[Title Page](#)[Abstract](#)[Introduction](#)[Conclusions](#)[References](#)[Tables](#)[Figures](#)[◀](#)[▶](#)[◀](#)[▶](#)[Back](#)[Close](#)[Full Screen / Esc](#)[Print Version](#)[Interactive Discussion](#)

EGU

**Tropospheric
distribution of
sulphate aerosol**

S. Verma et al.

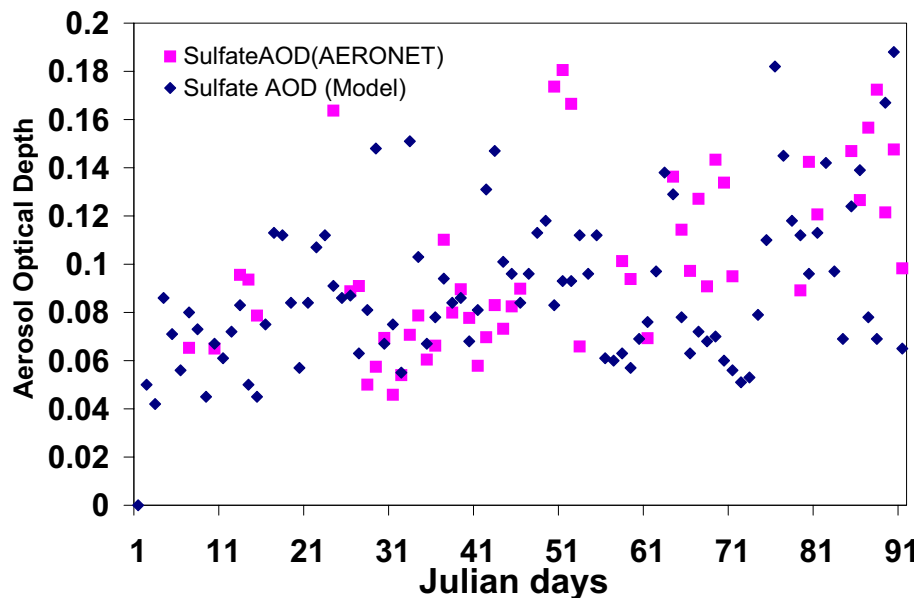


Fig. 3. Modelled and observed sulphate aerosol optical depth for the period January–March 1999 at Kaashidhoo [73.46° E, 4.96° N]. The observed AOD is obtained as 29% of the AERONET observed AOD. Note that rest of the figures are from SCN-RV except otherwise mentioned.

[Title Page](#)[Abstract](#)[Introduction](#)[Conclusions](#)[References](#)[Tables](#)[Figures](#)[◀](#)[▶](#)[◀](#)[▶](#)[Back](#)[Close](#)[Full Screen / Esc](#)[Print Version](#)[Interactive Discussion](#)

EGU

Tropospheric
distribution of
sulphate aerosol

S. Verma et al.

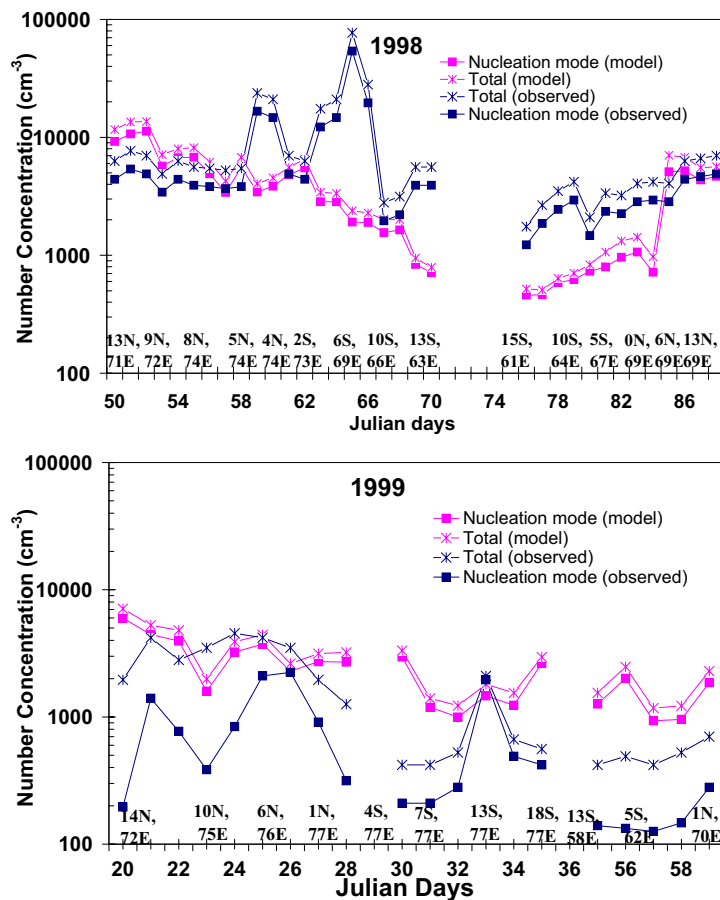


Fig. 4. Modelled and observed latitudinal variation of the total number and nucleation mode concentrations of sulphate aerosol particles along the cruise routes of FFP-98 and IFP-99. Observations are from Kamra et al. (2003) and are decreased by 30% for the sake of comparing with sulphate only modelled concentrations.

Title Page

Abstract

Introduction

Conclusions

References

Tables

Figures

◀

▶

◀

▶

Back

Close

Full Screen / Esc

Print Version

Interactive Discussion

**Tropospheric
distribution of
sulphate aerosol**

S. Verma et al.

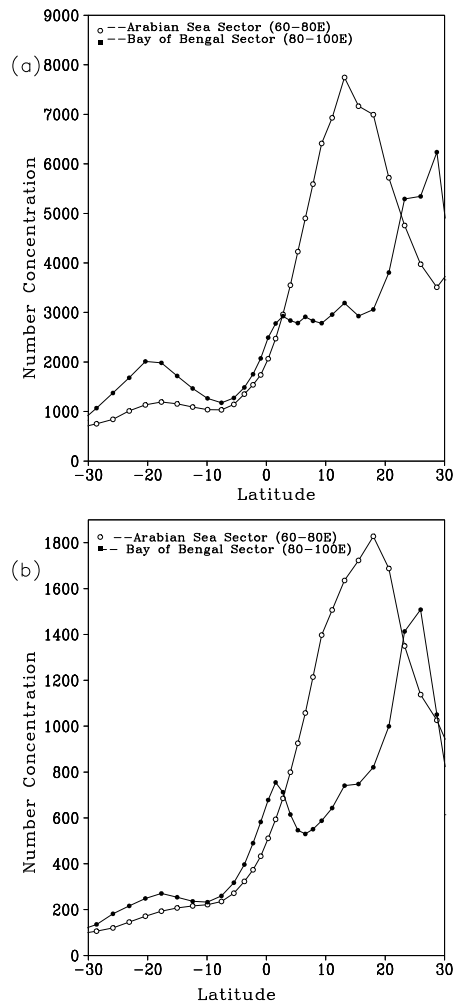


Fig. 5. Latitudinal variation of sulphate number concentration (particle cm^{-3}) in the **(a)** Aitken and **(b)** accumulation modes over the Bay of Bengal and Arabian Sea sectors.

[Title Page](#)[Abstract](#)[Introduction](#)[Conclusions](#)[References](#)[Tables](#)[Figures](#)[◀](#)[▶](#)[◀](#)[▶](#)[Back](#)[Close](#)[Full Screen / Esc](#)[Print Version](#)[Interactive Discussion](#)

EGU

Tropospheric
distribution of
sulphate aerosol

S. Verma et al.

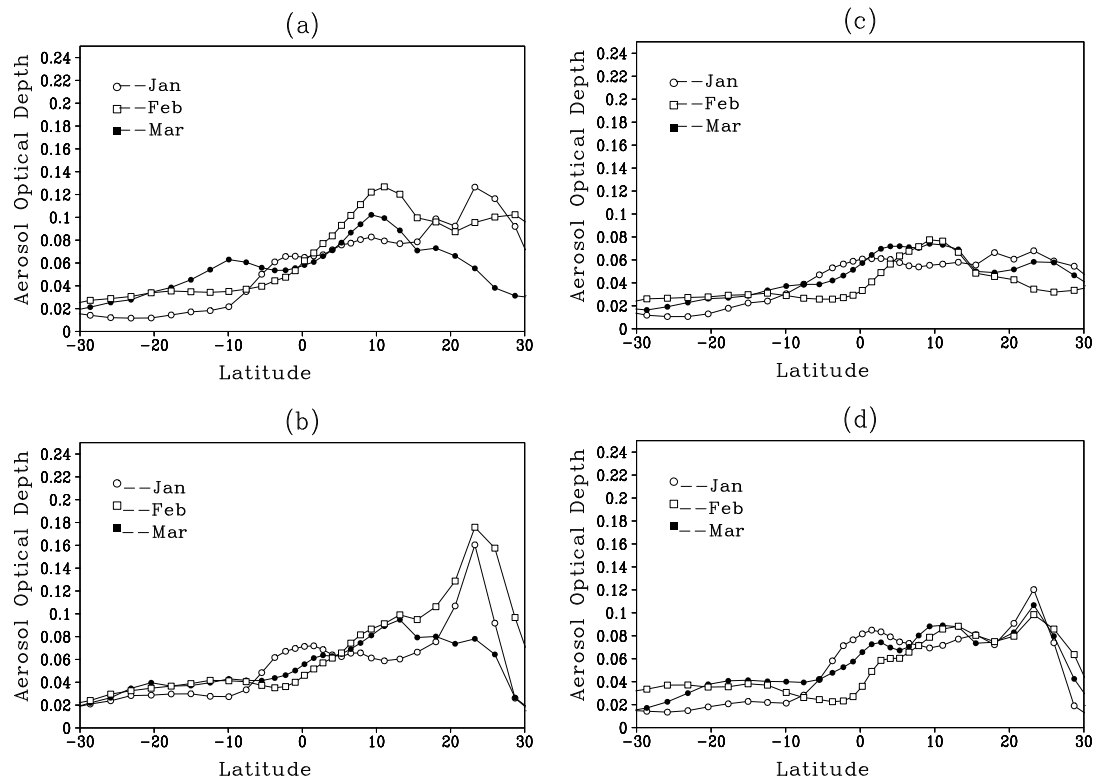


Fig. 6. Latitudinal variations of simulated sulphate AOD. **(a)** and **(c)** Arabian Sea sector (60° E–80° E), **(b)** and **(d)** Bay of Bengal sector (80° E–100° E). (a) and (b) are obtained from SCN-RV while (c) and (d) are from SCN-GEIA.

[Title Page](#)[Abstract](#)[Introduction](#)[Conclusions](#)[References](#)[Tables](#)[Figures](#)[◀](#)[▶](#)[◀](#)[▶](#)[Back](#)[Close](#)[Full Screen / Esc](#)[Print Version](#)[Interactive Discussion](#)

EGU

**Tropospheric
distribution of
sulphate aerosol**

S. Verma et al.

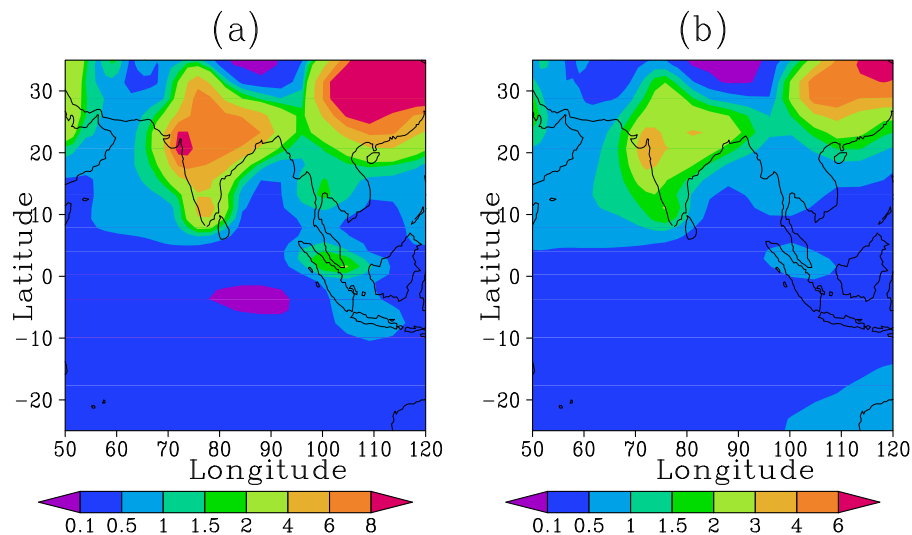


Fig. 7. Average SO₂ distribution for January to March 1999 for the INDOEX domain: **(a)** surface concentration ($\mu\text{g SO}_2 \text{ m}^{-3}$); **(b)** column burden (mg S m^{-2}).

[Title Page](#)[Abstract](#)[Introduction](#)[Conclusions](#)[References](#)[Tables](#)[Figures](#)[◀](#)[▶](#)[◀](#)[▶](#)[Back](#)[Close](#)[Full Screen / Esc](#)[Print Version](#)[Interactive Discussion](#)

EGU

Tropospheric
distribution of
sulphate aerosol

S. Verma et al.

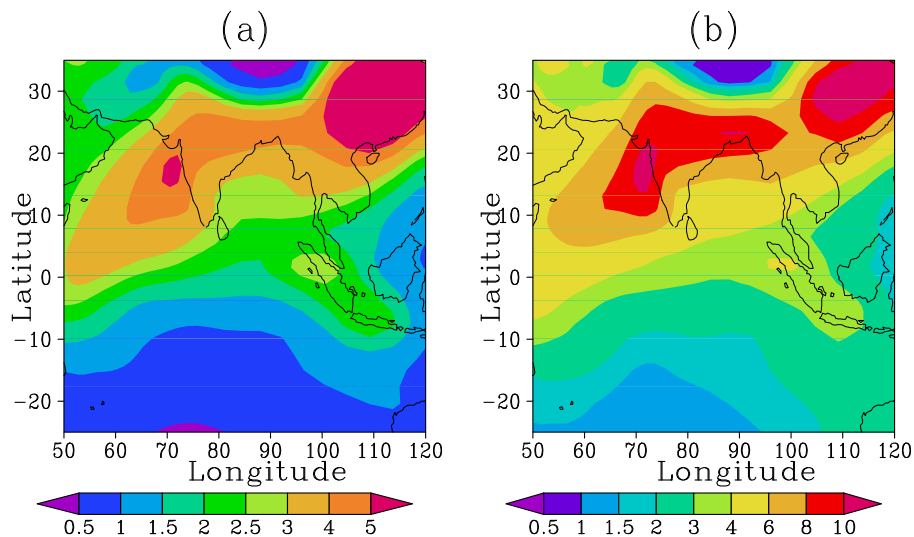


Fig. 8. Average sulphate distribution for January to March 1999 over the INDOEX domain: **(a)** surface concentration ($\mu\text{g SO}_4^{2-} \text{ m}^{-3}$); **(b)** sulphate column burden ($\text{mg SO}_4^{2-} \text{ m}^{-2}$).

[Title Page](#)[Abstract](#)[Introduction](#)[Conclusions](#)[References](#)[Tables](#)[Figures](#)[◀](#)[▶](#)[◀](#)[▶](#)[Back](#)[Close](#)[Full Screen / Esc](#)[Print Version](#)[Interactive Discussion](#)

EGU

**Tropospheric
distribution of
sulphate aerosol**

S. Verma et al.

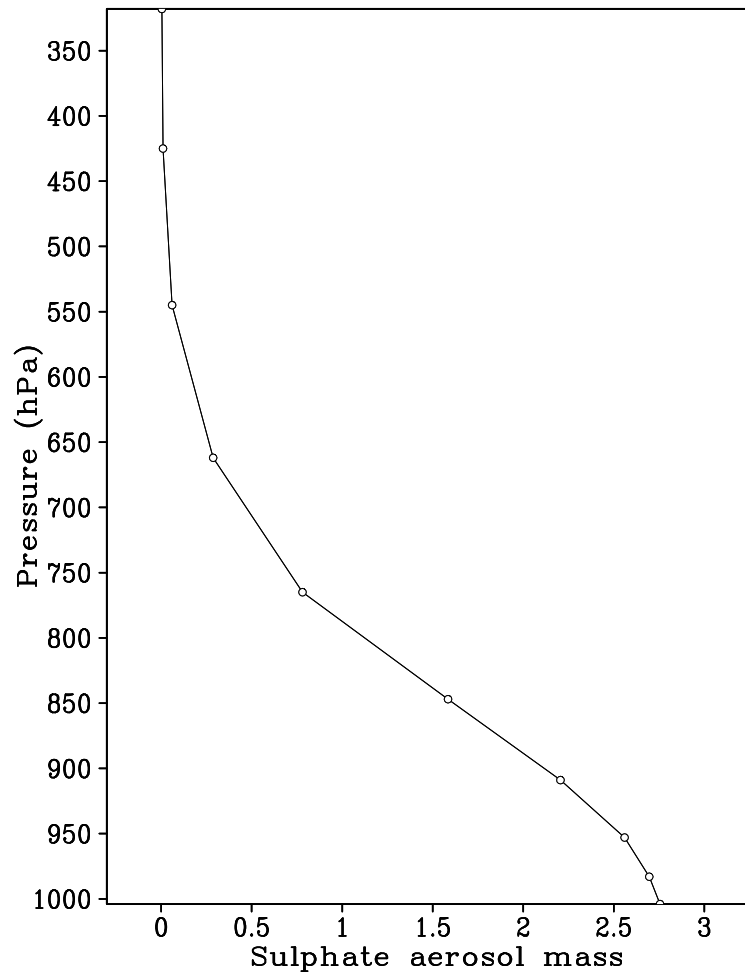


Fig. 9. Averaged vertical profile of sulphate aerosol mass ($\mu\text{g m}^{-3}$) over the entire INDOEX region for the IFF.

[Title Page](#)[Abstract](#)[Introduction](#)[Conclusions](#)[References](#)[Tables](#)[Figures](#)[◀](#)[▶](#)[◀](#)[▶](#)[Back](#)[Close](#)[Full Screen / Esc](#)[Print Version](#)[Interactive Discussion](#)

EGU

**Tropospheric
distribution of
sulphate aerosol**

S. Verma et al.

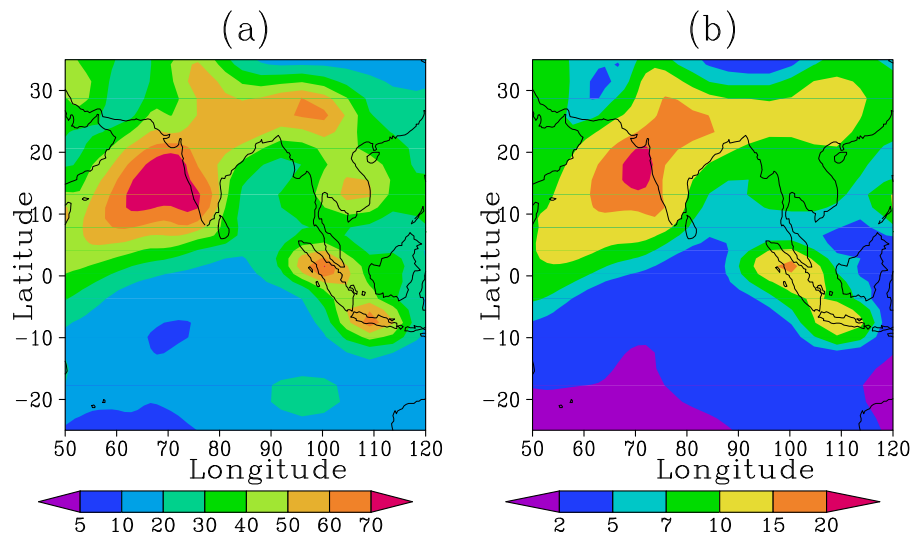


Fig. 10. Spatial distribution of particle number concentration (divided by 100) for January to March at surface in **(a)** Aitken mode and **(b)** accumulation mode concentration (particle cm^{-3}).

[Title Page](#)[Abstract](#)[Introduction](#)[Conclusions](#)[References](#)[Tables](#)[Figures](#)[◀](#)[▶](#)[◀](#)[▶](#)[Back](#)[Close](#)[Full Screen / Esc](#)[Print Version](#)[Interactive Discussion](#)

EGU

**Tropospheric
distribution of
sulphate aerosol**

S. Verma et al.

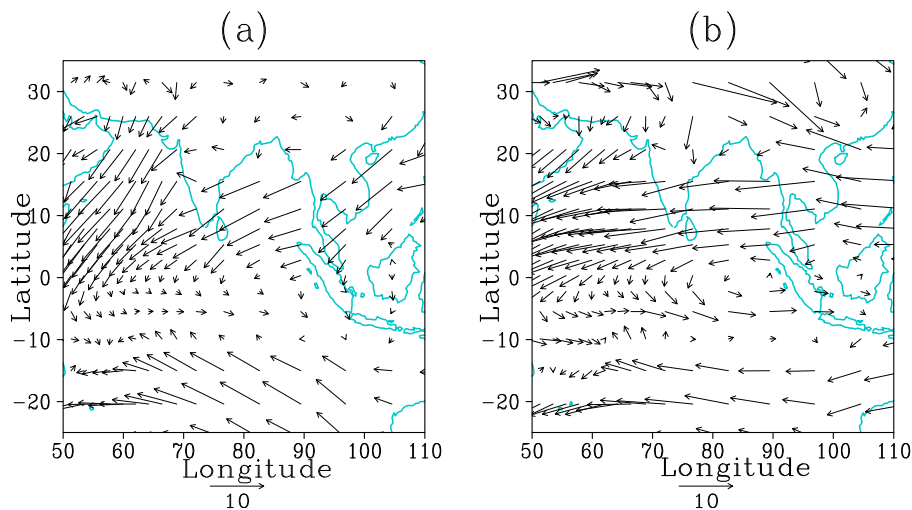


Fig. 11. Average wind field for January to March 1999 over the INDOEX domain at **(a)** the surface and **(b)** 850 hPa pressure level.

[Title Page](#)[Abstract](#)[Introduction](#)[Conclusions](#)[References](#)[Tables](#)[Figures](#)[◀](#)[▶](#)[◀](#)[▶](#)[Back](#)[Close](#)[Full Screen / Esc](#)[Print Version](#)[Interactive Discussion](#)

EGU

Tropospheric
distribution of
sulphate aerosol

S. Verma et al.

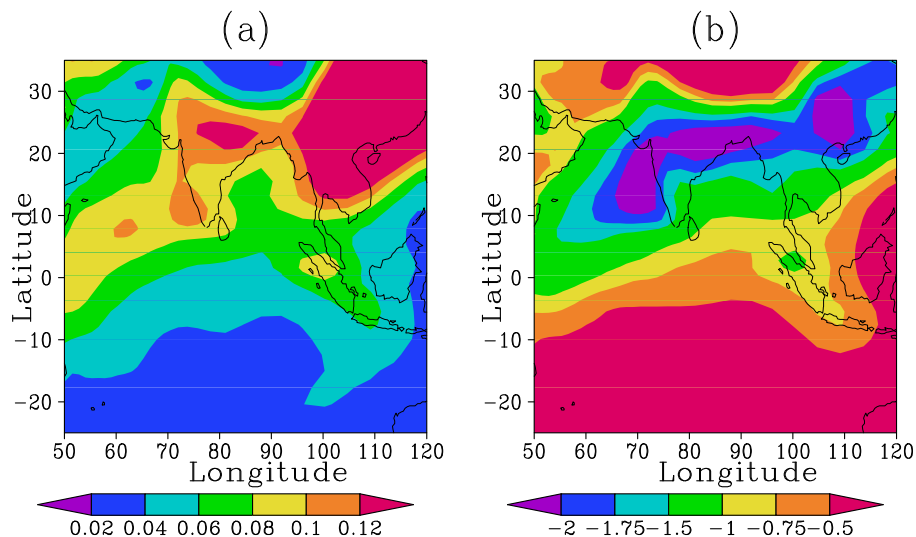


Fig. 12. (a) Sulphate aerosol optical depth during INDOEX-IFP, and (b) direct sulphate radiative forcing at top of atmosphere (Wm^{-2}).

[Title Page](#)[Abstract](#)[Introduction](#)[Conclusions](#)[References](#)[Tables](#)[Figures](#)[◀](#)[▶](#)[◀](#)[▶](#)[Back](#)[Close](#)[Full Screen / Esc](#)[Print Version](#)[Interactive Discussion](#)

EGU

**Tropospheric
distribution of
sulphate aerosol**

S. Verma et al.

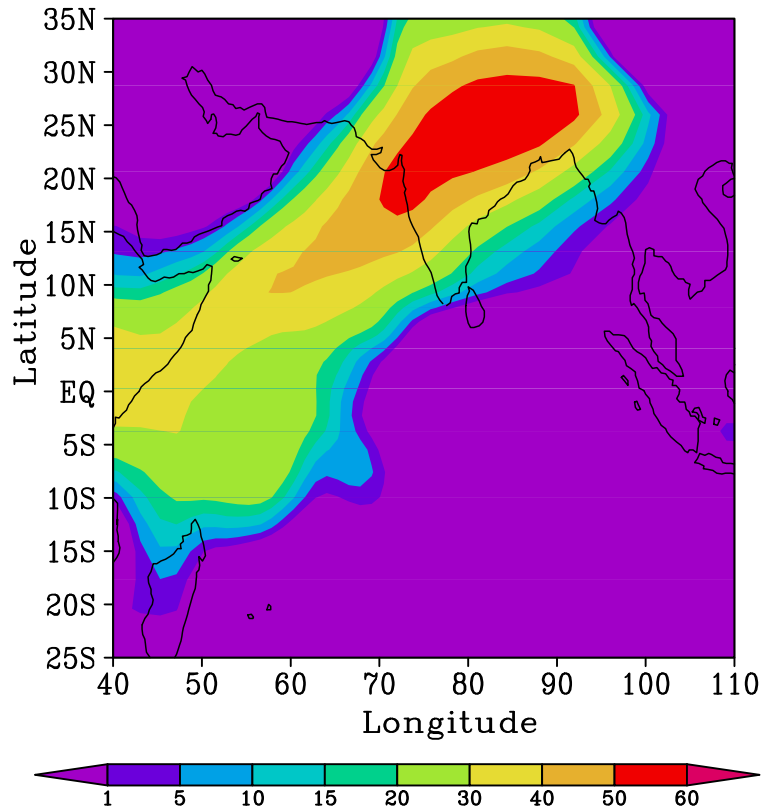


Fig. 13. Contribution (%) of the Indian sources to sulphate burden over the INDOEX region during the IFP.

[Title Page](#)[Abstract](#)[Introduction](#)[Conclusions](#)[References](#)[Tables](#)[Figures](#)[◀](#)[▶](#)[◀](#)[▶](#)[Back](#)[Close](#)[Full Screen / Esc](#)[Print Version](#)[Interactive Discussion](#)

EGU